Materials Science, *Vol. 21*, *No. 2*, *2003*

Intramolecular electron transfer on the vibrational timescale in mixed valence ruthenium clusters*

NAOYUKI IMAI, TOMOHIKO HAMAGUCHI, TADASHI YAMAGUCHI, AND TASUKU ITO**

Department of Chemistry, Graduate School of Science, Tohoku University, Sendai 980-8578, Japan

The thermodynamic stability of the mixed valence (one electron reduced) state between linked Ru_3 units was studied by means of electrochemical methods for the series of the ligand-bridged triruthenium cluster dimer, $[Ru_3(\mu_3\text{-}O)(\mu\text{-}CH_3CO_2)_6(CO)(L)(\mu\text{-}BL)Ru_3(\mu_3\text{-}O)(\mu\text{-}CH_3CO_2)_6(CO)(L)]$ (BL = 1,4-pyrazine: L = 4-dimethylaminopyridine (dmap) (**1a**), pyridine (py) (**1b**), 4-cyanopyridine (cpy) (**1c**), 1-azabicyclo[2.2.2]octane (**1d**); BL = 4,4′-bipyridine: L = dmap (**2a**), py (**2b**), cpy (**2c**); BL = 2,7-diazapyrene: L = dmap (**3a**); BL = 1,4-diazabicyclo[2.2.2]octane: L = dmap (**4a**), py (**4b**), cpy (**4c**)). The mixed valence states undergoing rapid intramolecular electron transfers were observed by IR spectro-electrochemistry. By simulating dynamical effects on the observed ν(CO) absorption bandshapes, the rate constants k_e for electron transfer in the mixed valence states of **1a**, **1b**, **1c** and **1d** were estimated to be 9×10^{11} s^{-1} (at room temperature (rt)), 5×10^{11} s^{-1} (at rt), *c.a.* 1×10^{11} s^{-1} (at rt), and 1×10^{12} s^{-1} (at –18 °C), respectively. Possible applications of this approach to asymmetric mixed valence systems were discusssed.

1. Introduction

Spectroscopic techniques for determination of molecular structure have their own timescales. As is well known, spectral coalescence in nuclear magnetic resonance (NMR) is on the order of milliseconds. In infrared (IR) spectroscopy, the timescale is on the order of picoseconds. Intramolecular processes such as electron and energy transfer can occur on the picosecond timescale. We recently reported our observations of coalescence of the C–O stretching bands of carbon monoxide (ν(CO)) ligands in the most rapidly exchanging mixed valence complexes of hexanuclear ruthenium clusters [1–3]. The mixed valence complexes are one-electron reduced species of ligand bridged dimers of triruthenium clusters of the $[Ru_3(\mu_3\text{-}O)(\mu\text{-}CH_3CO_2)_6(CO)(L)(\mu\text{-}BL)Ru_3(\mu_3\text{-}O)(\mu\text{-}CH_3CO_2)_6(CO)(L)]$ type, shown in Fig. 1, where BL denotes

* The paper was presented at the 13th Winter School on Coordination Chemistry, Karpacz, Poland, 9–13 December, 2002.

** Corresponding author, e-mail: ito@agnus.chem.tohoku.ac.jp.

bridging ligand. In the neutral isolated states of all the compounds, each trinuclear Ru_3 unit formally contains one Ru(II) and two Ru(III) centres and the carbonyl ligand is co-ordinated to the formally divalent centre. We describe the characteristics of the IR spectra of **1a–1d** and **2a–2b** along with electrochemical data of all the compounds shown in Fig. 1 [4]. Possible applications of infrared spectroelectrochemistry for the estimation of the rate constants of intramolecular electron transfer in asymmetric mixed valence system will also be discussed.

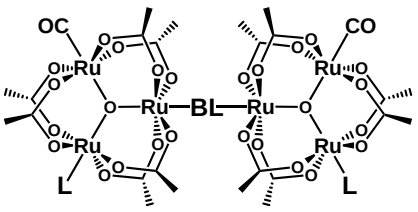

BL \ L	(dmap)	(py)	(cpy)	(abco)
(pz)	**1a**	**1b**	**1c**	**1d**
(bpy)	**2a**	**2b**	**2c**	—
(dap)	**3a**	—	—	—
(dabco)	**4a**	**4b**	**4c**	—

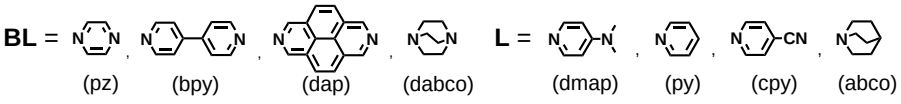

Fig. 1. Structure of $[Ru_3(\mu_3\text{-}O)(\mu\text{-}CH_3CO_2)_6(CO)(L)(\mu\text{-}BL)Ru_3(\mu_3\text{-}O)(\mu\text{-}CH_3CO_2)_6(CO)(L)]$ and numbering of the compounds: pz – 1,4-pyrazine, bpy – 4,4′-bipyridine, dap – 2,7-diazapyrene, dabco – 1,4-diazabicyclo[2.2.2]octane, abco – 1-azabicyclo-[2.2.2]octane

2. Electrochemically generated mixed valence states and their thermodynamic stabilities

Figure 2 shows cyclic voltammograms (CV) of a series of Ru_3 dimers where the bridging ligand is fixed to pyrazine and the terminal ligands are varied. Figure 3 shows CV's of a series of Ru_3 dimers where the bridging ligand is varied and the terminal ligand is fixed to dmap. In all the CV's in Figs. 2 and 3, two-electron oxidation waves are observed at approximately $E_{1/2}(2/0) = 0.50$ and $E_{1/2}(4/2) = 1.3$ V vs. SSCE. Here, the overall charges of the complexes are expressed in parentheses. On the other hand, each compound generally displays two single electron reduction waves that correspond formally to $Ru_3^{III,III,II}$-BL-$Ru_3^{III,III,II}$/$Ru_3^{III,III,II}$-BL-$Ru_3^{III,II,II}$ (0/–1) and then $Ru_3^{III,III,II}$-BL-$Ru_3^{III,II,II}$/$Ru_3^{III,II,II}$-BL-$Ru_3^{III,II,II}$ (–1/–2). In the case of **4a**, the splitting between the (0/–1) and (–1/–2) states is too small ($\Delta E \approx 0$ mV) to resolve by cyclic voltammetry. One important contribution to the magnitude of the splitting between the single electron (0/–1) and (–1/–2) reduction waves, ΔE, is the stabilization energy imparted to the –1 state by electron delocalization. Comproportionation constants, $K_c = \exp(\Delta EF/RT)$, estimated from ΔE are also given in Figs. 2 and 3. The mixed valence species, i.e., the –1 state exists in the region of ΔE between the (0/–1) and (–1/–2) waves and the magnitude of ΔE, and thereby K_c, reflects stability of the mixed valence state. Redox potential data for the (0/–1) and (–1/–2) processes are summarized in Table 1.

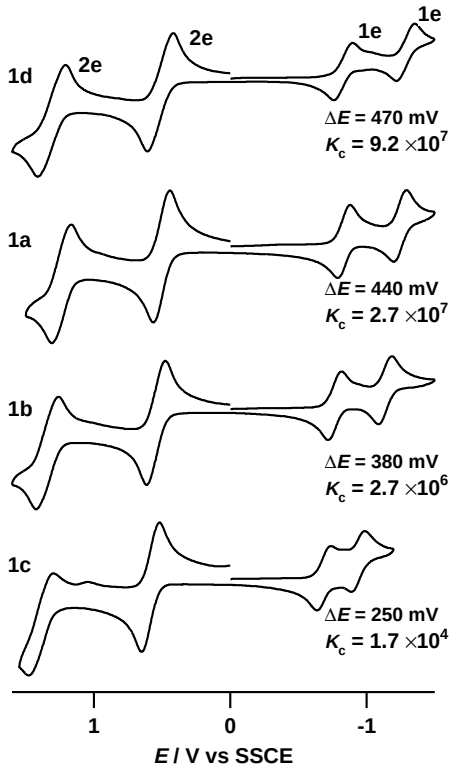

Fig. 2. Cyclic voltammograms, ΔE, and K_c of $[\{Ru_3(\mu_3\text{-}O)(\mu\text{-}CH_3CO_2)_6(CO)(L)\}_2(\mu\text{-}pz)]$ (L = abco (**1d**), dmap (**1a**), py (**1b**), cpy (**1c**))

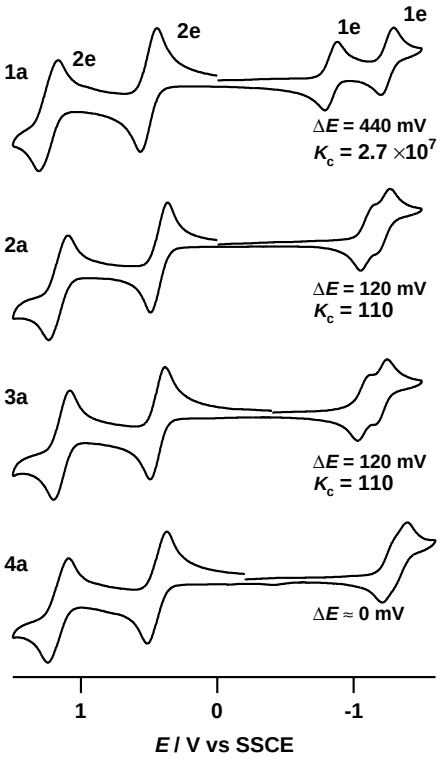

Fig. 3. Cyclic voltammograms, ΔE, and K_c of $[\{Ru_3(\mu_3\text{-}O)(\mu\text{-}CH_3CO_2)_6(CO)(dmap)\}_2(\mu\text{-}BL)]$ (BL = pz (**1a**), bpy (**2a**), dap (**3a**), dabco (**4a**))

Table 1. Electrochemical data for $[\{Ru_3(\mu_3\text{-}O)(\mu\text{-}CH_3CO_2)_6(CO)(L)\}_2(\mu\text{-}BL)]$

Compound	BL	L	$E_{1/2}(0/-1)$[a], V	$E_{1/2}(-1/-2)$[a], V	ΔE (mV)	K_C
1a	pz	dmap	–0.89	–1.33	440	2.7×10^7
1b	pz	py	–0.81	–1.19	380	2.7×10^6
1c	pz	cpy	–0.68	–0.93	250	1.7×10^4
1d	pz	abco	–0.84	–1.31	470	9.2×10^7
2a	bpy	dmap	–1.11	–1.23	120	1.1×10^2
2b	bpy	py	–1.03	–1.11	80	2.3×10^1
2c	bpy	cpy		–0.91(2e)	≈0	<10
3a	dap	dmap	–1.08	–1.20	120	1.1×10^2
4a	dabco	dmap	–1.25	–1.31	60	3×10^1
4b	dabco	py	–1.12	–1.17	50	7×10^0
4c	dabco	cpy		–0.94(2e)	≈0	<10

[a]Cyclic voltammograms recorded in 0.1 M tetra-*n*-butylammonium hexafluorophosphate in dichloromethane, V versus saturated sodium chloride calomel electrode (SSCE).

An interesting aspect of these complexes is that the splitting ΔE depends strongly on the ancillary ligands (dmap, py, cpy, abco) and on the bridging ligands (pz, bpy, dap, dabco). Thus, as the adjustable pyridyl ligand in the series **1a–1c** and **2a–2c** is changed from dmap in **1a** and **2a** to an unsubstituted pyridine for **1b** and **2b** to an electron withdrawing cpy for **1c** and **2c**, the values of ΔE and K_c decrease considerably (Table 1). Compound **1d** with abco, which has the largest pK_a of 11.1 among the present series of terminal ligands, possesses the largest ΔE and K_c [4]. The bridging ligand π-electron systems mediate electronic coupling between the two Ru_3 centres, and the overlap between the Ru_3 cluster dπ-electron system and the bridging ligand π^* system appears to be very favourable. In fact, the dabco bridged compound **4a**, which has no π-electron system in the bridging ligand, shows essentially no electronic coupling ($\Delta E \approx 0$). The relevant Ru d level is closer to the pz π^* level in **1a** than it is in **1c**, and closer to the bpy π^* level in **2a** than it is in **2c**. This description of the electronic structure is supported by experimental evidence [2]. In general, electronic coupling falls off exponentially with increasing distance between electronically interacting centres. The centre-to-centre separation between Ru_3O units in the crystal structure of **1a** is 10.9 Å [5], and it is estimated at ca. 15.3 Å in bpy bridged complexes. The longer separation between Ru_3 centres in **2a–2c** and **3a** decreases the intercluster electronic coupling, thereby decreasing ΔE values.

3. IR Spectra of the mixed-valence species in the ν(CO) region

The vibrational spectra of complexes **1a–1d** and **2a–2c** were obtained by using reflectance IR spectroelectrochemistry (SEC). Controlled potentials were applied to prepare the singly (–1) and doubly (–2) reduced states of cluster for IR spectroscopic observation. Measurements were carried out at room temperature unless otherwise stated. Experiments on **1d** were carried out at –18 °C, because reduced species (the –1 and –2 states) of this compound were unstable at room temperature. Figures 4a and b show the IR spectra in the ν(CO) region of pyrazine (**1a–1d**) and 4,4′-bipyridine (**2a–2b**) bridged complexes. Let us discuss first the pyrazine bridged systems. In the isolated (0) state, **1d** exhibits a single ν(CO) band at 1937 cm^{-1} (Fig. 4a top), indicating that two Ru_3 units in **1d** are pairwise equivalent. The doubly reduced species also gives rise to a single ν(CO) band, but at 1890 cm^{-1}, reflecting identical redox states at each $Ru_3^{III,II,II}$ cluster. Complexes **1a–1c** similarly exhibit single ν(CO) bands in the neutral state and –2 state, respectively. Interestingly, however, the single-electron reduced state of **1d** shows a broad absorption band at the average energy of the bands observed for the neutral (0) and doubly reduced (–2) states of **1d** (Fig. 4a top). The degree of 'coalescence' of the IR spectra depends on the degree of electronic coupling between the pyrazine-linked Ru_3 clusters (Fig. 4a). As ΔE (or K_c) decreases from 470 mV (9.2×10^7) for **1d** to 250 mV (1.7×10^4) for **1c**, two distinct ν(CO) bands at 1931 cm^{-1} and 1904 cm^{-1} become resolved for **1c**. Cluster **1b** with an intermediate

value of ΔE (K_c) of 380 mV (2.7×10^6) shows an intermediate degree of spectral 'coalescence' in the singly reduced state.

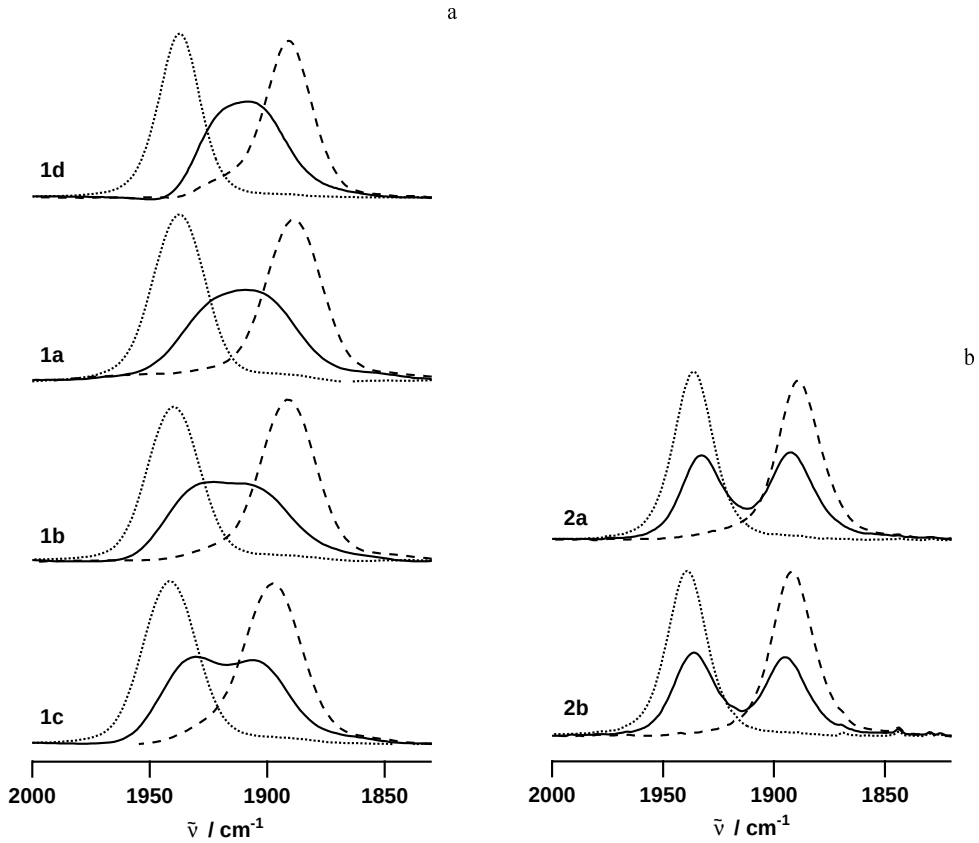

Fig. 4. IR spectra in the ν(CO) region for: a) $[\{Ru_3(\mu_3\text{-}O)(\mu\text{-}CH_3CO_2)_6(CO)(L)\}_2(\mu\text{-}pz)]^{n+}$ (n = 0 (···), -1 (—), –2 (- - -)) for L = abco (**1d**), dmap (**1a**), py (**1b**), cpy (**1c**); b) $[\{Ru_3(\mu_3\text{-}O)(\mu\text{-}CH_3CO_2)_6(CO)(L)\}_2(\mu\text{-}bpy)]^{n+}$ (n = 0 (···), –1 (—), –2 (- - -)) for L = dmap (**2a**), py (**2b**)

Similarly, both the neutral and –2 states of the bpy bridged complexes **2a–2c** exhibit one sharp ν(CO) band in the IR (Fig. 4b). The spectra of the –1 states of **2a** and **2b** consist of two well-resolved and well-separated ν(CO) bands, perturbed only slightly relative to the spectra of the neutral and –2 states. For **2c**, a reliable spectrum of the –1 state could not be obtained due to < 50 mV separation between the (0/–1) and (–1/–2) CV waves. In clusters **2a–2c**, the electronic coupling is small as evidenced by cyclic voltammetry. Overall, the singly reduced states of **2a–2c** can be viewed as valence trapped or localized compounds.

The IR spectral feature in the ν(CO) region of the –1 mixed valence state is very different between pyrazine bridged complexes **1a–1d** and 4,4′-bipyridine complexes

2a–2c. The vast difference in spectral characteristics arises from the electronic interactions between two Ru_3 units through the bridging ligand, as is seen in their electrochemical behaviour. The use of longer bpy bridges in **2a–2c** attenuates the electronic coupling to the point that in **2c** the –1 charge transfer state is no longer defined. Preliminary experiments show essentially no temperature dependence of the IR spectra in the range from room temperature down to –40 °C.

4. Estimation of rate constants of intramolecular electron transfer in the mixed valence state

At the present time, we have no evidence of a process other than intramolecular electron transfer to account for the changes observed in the IR spectral line shapes of our systems. We carried out the Bloch equation type analysis for the IR line broadening which is developed by McClung [6].

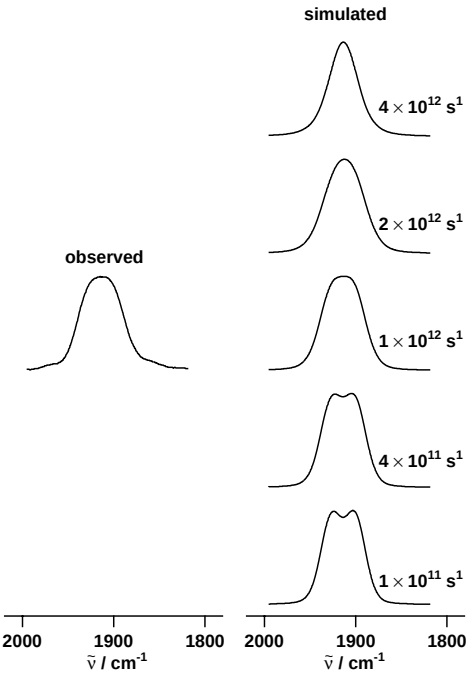

Fig. 5. Comparison of observed to simulated infrared spectra in the ν(CO) region for $\mathbf{1a}^-$ as a function of the intramolecular electron transfer rate constant k_e

Figure 5 shows an example of the simulated spectral line shapes as a function of the rate constant k_e and a comparison to the observed spectrum of $\mathbf{1a}^-$. Similar analyses were carried out for $\mathbf{1a}^-$–$\mathbf{1c}^-$ and $\mathbf{2a}^-$ [2]. The rate constants k_e of electron transfer

estimated by this type of simulation for **1d**$^-$, **1a**$^-$, **1b**$^-$, and **1c**$^-$ are (10±2)×10^{11} at −18 °C, (9±3)×10^{11}, (5±3)×10^{11}, ca. 1×10^{11} s^{-1}, respectively. Simulated spectra as a function of k_e for **1c**$^-$ show that k_e for **1c**$^-$ is close to the lower limit that can be determined reliably by this approach [2].

5. Possible applications of IR SEC for the estimation of the rate constants of intramolecular electron transfer in asymmetric mixed valence state

Using different terminal ligands at the L^1 and L^2 sites, we can prepare a series of asymmettric Ru_3 dimers **1e–1g** (Fig. 6). They show CV similar to the symmetric Ru_3 dimers **1a–1d**, giving redox wave splitting ΔE (410, 310, and 350 mV for **1e**, **1f**, and **1g**, respectively). The mixed valent −1 states of **1e–1g** also show similar intervalence transition band (at 11,500; 10,500; and 10400 cm^{-1}, for **1e**, **1f**, and **1g**, respectively). These observations strongly suggest a possible application of the above-mentioned technique to asymmetric mixed valence systems.

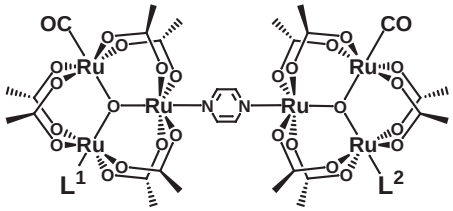

	L^1	L^2
1e	dmap	py
1f	py	cpy
1g	dmap	cpy

Fig. 6. Structure of asymmetric dimer[$Ru_3(\mu_3\text{-}O)(\mu\text{-}CH_3CO_2)_6(CO)(L^1)(\mu\text{-}pz)Ru_3(\mu_3\text{-}O)(\mu\text{-}CH_3CO_2)_6(CO)(L^2)$] and numbering of the compounds.

In contrast to the symmetric system, however, intramolecular electron transfer in the asymmetric system is somewhat complicated. A comparison of potential energy surface for symmetric and asymmetric mixed valence system is shown in Fig. 7.

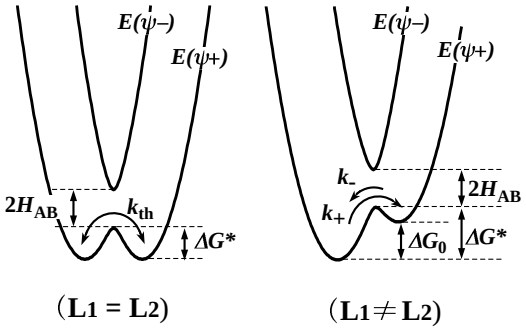

Fig. 7. Potential surfaces for symmetric and asymmetric systems

The question of whether such an asymmetric mixed valence state undergoes intramolecular electron transfer (localized or delocalized) depends on two factors: (1) the potential difference, ΔG_0, and (2) the electronic coupling, H_{AB}. Larger contributions of H_{AB} tend to delocalize the system, whereas a larger ΔG_0 tends to localize the system. When H_{AB} and ΔG_0 are of appropriate magnitude, two mixed valence isomers should exist where one is a major isomer and the other a minor one, and intramolecular electron transfer occurs within each isomer. The intramolecular electron transfer in the major isomer results in the formation of the minor isomer and *vice versa*. Thus far, this behaviour in an asymmetric mixed valence state has not been reported to our best knowledge. We found preliminarily that one electron reduced forms of the asymmetrically substituted dimers of ruthenium trimers, **1e–1g**, exhibit the above-mentioned asymmetric mixed valence behaviour: major and minor species in a single mixed valence state exist, and intramolecular electron transfer causes infrared line coalescence in the ν(CO) region. A detailed study is now in progress.

6. Conclusions

There are uncertainties in the rates of electron transfer estimated by Bloch equation simulation of the IR band shape. The precise relationship between IR line shape and electron-transfer dynamics still needs to be refined. But IR band coalescence phenomena observed in this study suggest that intramolecular electron transfer does occur on the IR timescale and offers great advantages for comparing theory and experiment.

Acknowledgment

This work was supported by Grants-in-Aid for Scientific Research (Priority Areas No. 10149102 'Metal-assembled Complexes') and for International Scientific Research (Joint Research No. 11694051) from the Ministry of Education, Science, and Culture, Japan. We also thank collaborators given in the references.

References

[1] ITO T., HAMAGUCHI T., NAGINO H., YAMAGUCHI T., WASHINGTON J., KUBIAK C.P., Science, 277 (1997), 660.
[2] ITO T., HAMAGUCHI T., NAGINO H., YAMAGUCHI T., KIDO H., ZAVARINE I .S., RICHMOND T., WASHINGTON J., KUBIAK C. P., J. Am. Chem. Soc., 121 (1999), 4625.
[3] Ito T., YAMAGUCHI T., KUBIAK C.P., Macromol. Symp., 156 (2000), 269.
[4] YAMAGUCHI T., IMAI N., ITO T., KUBIAK C.P., Bull. Chem. Soc. Jpn., 73 (2000), 1205.
[5] unpublised result.
[6] GREVELS F.-W, KERPEN K., KLOTZBUCHER W.E., MCCLUNG R.E.D., RUSSEL G., VIOTTE M., SCHAFFNER K., J. Am. Chem. Soc., 120 (1998), 10423.

Received 10 April 2003
Revised 17 April 2003